This article has been accepted for publication in a future issue of this journal, but has not been fully edited. Content may change prior to final publication. Citation information: DOI 10.1109/TWC.2019.2921964, IEEE Transactions on Wireless Communications

Body-Guided Galvanic Coupling Communication for Secure Biometric Data

William J. Tomlinson*, Stella Banou*, Shay Blechinger-Slocum*, Christopher Yu**, and Kaushik R. Chowdhury*

*Northeastern University, Boston MA, USA, Email: {wjtomlin, sbanou, sblechin, krc}@ece.neu.edu

**Draper Laboratory, Cambridge MA, USA, Email: cyu@draper.com

Abstract

In a world dominated by wearable IoT devices, malicious security threats have become a common concern in system design. Guided by this notion, we propose a secure transmission system through body-guided channels using Galvanic Coupling (GC). The GC-method injects weak electrical current into human tissue, primarily propagating through the skin. The proposed design provides impermeability to malicious attacks, (e.g. side-channel sniffing) when sending biometric data, as the body behaves as a natural waveguide. The following contributions are: (i) Analytical formulation and empirical verification of a 3D tissue equivalent circuit model for GC-signal propagation of the human arm-wrist-palm channel, (ii) Simulation study of numerous modulation schemes, drawn from the validated results of the GC-channel model, (iii) The design and implementation of a transceiver prototype using optimal communication parameters (modulation, frequency, power) for transmission on a dielectrically equivalent tissue phantom, and (iv) through experimental trials, we demonstrate the eavesdropping susceptibility of GC-signals, and similar body communication techniques, over-the-air and while in direct contact with the medium. Performance results of the GC-transceiver prototype yield a bit error rate of 10^{-6} with a transmit power of -2 dBm, in addition to over 7x reduction of signal radiation outside the body compared to capacitive coupling.

I. Introduction

With the expansion of the wearable technology ecosphere, the pervasiveness of the Internet of Things (IoT), and more recently, the *tactile* IoT, are enabling the human-in-the-loop in

This article has been accepted for publication in a future issue of this journal, but has not been fully edited. Content may change prior to final publication. Citation information: DOI 10.1109/TWC.2019.2921964, IEEE Transactions on Wireless Communications

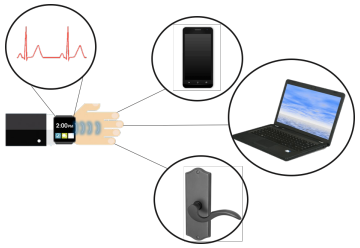

Fig. 1: A biological signal is acquired by a wrist-worn device and transmitted through the human skin to unlock devices by physical contact.

unprecedented ways. From body worn sensors to actively controlling smartphones via touch inputs, we continuously communicate large amounts of personal data with the outside world. The prevalent secure communication methods rely on antiquated biometrics or the transmission of secure keys through wireless channels. However, as we argue next, these forms of inputs can be easily spoofed and are highly susceptible to intentional eavesdropping and privacy-manipulation enabled by off-the-shelf but sophisticated software defined radios. Instead of using an over-the-air channel and traditional biometrics, we propose a radically different communication pathway to transmit biological signals containing advanced biometric information collected (via on-body sensors) in real-time. Our approach uses on-skin conduction through a technique called galvanic coupling (GC), where weak electrical currents are modulated with information and then injected into the human tissue [1].

•**Limitations of existing biometrics and passwords:** Despite the ubiquitous use of biometrics like fingerprints, retina/iris and facial features for commercial use, mobile devices still utilize auxiliary passwords for additional forms of secure communication. The use of traditional passwords often yields drawbacks in terms of user recollection, password strength and scale. Fingerprints, although unique, are transferable and can be left on various surfaces that users have daily interaction with. Such vulnerabilities are exploited via plastic, latex or gelatin based molds, used to forge a copy of the individuals biometric. Additionally, high resolution images/videos are used in counterfeiting retina and facial recognition software [2]. Hence, we believe that a new class of biophysical signals drawn from within the user's own body, such as the well-known electrocardiogram (ECG) signal [3], can yield high levels of individual distinction [4] and have found increasing use in secure communication [5]. Capturing and relaying these signals to an external point remains an open challenge, which we propose to tackle in this paper.

•**Limitations of over-the-air RF:** Although research on key generation and sharing for wireless sensors have made rapid strides, increasingly sophisticated sniffing attacks, coupled with limited computational resources within the sensors, pose practical limitations [2]. Instead, we propose an alternate method of transmitting information securely using GC that bypasses the vulnerable RF transmission channel. GC uses weak electrical current (0.5mA) that is modulated by the information to be transmitted. This data carrying signal is coupled to the body tissue, here the skin surface, by simple, small form-factor electrodes. By setting the operating frequency in the range 100kHz-1MHz, the signal energy is largely retained within the human tissue. Thus, with negligible amount of external radiation, it mitigates sniffing attacks. The only way to intercept the signal is to physically touch the subject with a pair of receiving electrodes.

•**Galvanic vs Capacitive Coupling:** Coupling based intra-body communication is classified into two types based on the nature of propagation. The first method, which we utilize in this work, is known as Galvanic Coupling (waveguide based). The second, Capacitive Coupling (electric-field based), also employs a pair of electrodes at the transmitter and receiver terminals [6]. In the GC method, both transmitter and receiver electrodes are attached to the body (with individual references) and alternating current is injected differently between the transmitter electrodes. A dominant source of current will flow between the positive and negative terminals of the transmitter, but a weaker, secondary current will flow throughout the tissues where the receiver electrodes will measure the potential difference across them [7]. In the Capacitive Coupling (CC) method, the signal electrode of the transmitter and the receiver are typically attached (or placed in close proximity) to the human body while the ground electrodes are floating, thereby capacitively coupling the human body to its surrounding environment. The signal electrode of the transmitter induces an electric field into the human body. The induced electrical signal is controlled by an electrical potential and the body acts as a floating conductor with the ground as the return path [8]. Unfortunately, this behavior makes capacitive coupling more susceptible to motion and external interference (e.g., power line, objects with conducting surfaces and potentially neighboring capacitively coupled body networks) [9]. Galvanic coupling signals, although more sensitive to body locations, body composition, electrode orientation and inter-electrode distances, are confined within the human tissue layers and thus are virtually unaffected by outside environmental conditions [7]. We exploit this feature to enable secure side-channel communication for the transmission of biometric data.

•**Galvanic Coupling Equivalent Circuit Channel Modeling:** Extensive work has been done

in [1], [10] to analytically model the human body channel as a complex network of impedances, representing the different layers of human tissue and their boundaries. For example, in [1], each layer of human tissue is modeled as combination of electrical circuits that constitute a 2-port network for the computation of signal gain at an output terminal. The implementation of the 2-port circuit model allows easy modification of parameters (center frequency, electrode separation, electrode dimensions, etc.) and flexibility in terms of transmitter and receiver placement. Previous methods of channel modeling, although highly complex and well inclusive of the dielectric properties of human tissue, assume uniformity across all signal paths and tissue layers, such as an end-to-end propagation cross-section as a single, homogeneous medium. Therefore, the channel modeling conducted in this work focuses on a 3D tissue equivalent circuit model with varying dimensions that adequately reflect the portion of the body used as a communication medium.

•**Galvanic Coupling Communication Systems:** Experimental platforms and testbeds using GC have been proposed in [11], [12]. In [11] differential binary phase-shift-keying (DBPSK) modulation is selected given its robustness to amplitude variations and minimal hardware complexity when compared to coherent schemes. The work conducted in [12] proposes a pulse position modulation ultra wideband system and follows the specifications of the physical layer outlined in IEEE 802.15.6 for Wireless Body Area Networks. However, these systems offer macro-scale representations of the transmitter and/or receiver architecture, characteristics not yet applicable for the wearable device arena. Additionally, there is no example application with packet-level framing of data demonstrated earlier, as the main focus is to conduct empirical analysis to verify channel behavior. In contrast, our work focuses on the sending and receiving of biological data via GC, with a system design focused on operation in the wearable domain.

•**Body-Guided Authentication Systems:**

In the commercial space, the Nymi Band [5] is a wearable authenticator designed to work with other devices (desktop computers, doors, etc.) and perform authentication based on proximity to the locked device. The Nymi band employs a biological signal (e.g., Lead I ECG measurements) as a biometric. Once a user is authenticated, it uses Bluetooth Low Energy and NFC to pair with devices running the Nymi supported application. The works presented in [13] and [14] enable continuous authentication with commodity devices using capacitive coupling body communication. Specifically, [13] proposes an impedance measurement biometric system with a touch sensing mechanism. This data is modulated through the user's body using an On-Off Keying

This article has been accepted for publication in a future issue of this journal, but has not been fully edited. Content may change prior to final publication. Citation information: DOI 10.1109/TWC.2019.2921964, IEEE Transactions on Wireless Communications

approach. Additional CC-based examples of touch based authentication systems are listed in [8], where a wrist-worn tag, containing a unique ID key, exchanges information with a receiver through touch. Similarly, the work in [15] and [16] present a touch enabled body communication system for multimedia-based applications by encoding information on captured touch instances and electromagnetic interference data, respectively. The above-mentioned studies show great potential for using biological data as a biometric and the utility of proximity/touch-based communication for authentication. However, all the above wireless communication methods using classical RF or CC still operate over-the-air, and thus are susceptible to eavesdropping, data interception, or data/fault injection (as we show later in Section V). To the best of our knowledge, the only system that employs GC for the transmission of biometric data can be found in [17]. Thus, we are motivated to develop a secure GC-based surface-to-surface communication by avoiding the over-the-air medium and mitigating the effects of contact-based susceptibility.

•**Proposed Approach: Secure biometric transmission with GC:** Our proposed system, envisioned in Figure 1, is composed of a wearable (here, we show a specific use-case for the upper forearm band that allows transmission of ECG signals, though any other signal/body location can be chosen), as opposed to intrusively implanting devices that are not required for improving one's quality of life. The device non-invasively acquires a biological signal, extracts unique features and modulates a weak electric current to create the non-radiating GC-waveform. This GC-signal is transmitted wirelessly through the arm, wrist and palm of the subject to the receiver, be it a data logging entity, actuation interface (e.g., door handle) or a smart-device. The receiver has a GC front-end that captures the signal and then feeds it to a classifier for pattern matching.

The main contributions of our work are as follows:

1) We design and experimentally validate an electrically-equivalent circuit model of the human arm-wrist-palm tissue channel and characterize the behavior of the GC-signal. We use the results of our channel studies to optimize the design of transmission parameters and modulation schemes for the galvanic coupling communication system.
2) Through experimental evaluation, we show how the GC-signal emits minuscule levels of signal radiation outside the body compared to the well-studied Capacitive Coupling (CC) and similar solutions for body-guided communication. Furthermore, we show that our use of the GC-signal makes it virtually unfeasible to decode data over-the-air at an adversarial receiver.
3) We evaluate the impact of an adversarial receiver when in contact with the surface of the

human body channel, demonstrating that results do not produce a significant increase in eavesdropping advantage when compared to over-the-air side-channel attacks.

4) We present a method for identifying disadvantageous changes in channel behavior, brought on by direct contact to the human body channel during data transmission, and provide an analysis of the suitable FEC schemes that mitigate a loss in link performance.
5) We implement a proof-of-concept secure biometric transmission system using the Teensy^{TM} microcontoller unit that supports analog front-end hardware for transmission and reception of GC-signals.
6) We measure the achievable energy consumption metrics and demonstrate the link performance of our prototype by transmitting sample ECG data (provided by PhysioNet [18]) with a bit-error-rate (BER) of 10^{-6} and a transmit power of -2 dBm. Moreover, all data files and software code are available to the community for repeatability of experiments.

II. GC Channel Model for Arm-Wrist-Palm

Our approach relies on a carefully tuned physical layer design optimized with respect to the arm-wrist-palm path that is employed to relay biometric information. This is a generic pathway, which can be adapted for other tissue segments. We depart from the assumption of tissues resembling homogeneous cylinders in [1], but we retain the concept of creating an electrical equivalent circuit. Key assumptions that we make in this work (also validated later through experiments) are: (i) the section of the arm where the biometric signal is retrieved, and then forwarded through the wrist area, is cuboidal in shape; and (ii) the thickness and properties of each tissue layer, i.e., skin, fat, tendon, muscle, bone are uniform within the separate partitioned segments that form the arm, wrist and palm.

We separately analyze the propagation from the three parts of the path: the arm, wrist and palm. We first begin by identifying typical tissue thickness and propagation characteristics of each of these three segments. For example, a segment consists of four layers: skin, fat, muscle and bone for the arm and skin, fat, tendon and bone for the wrist (Figure 2). Through cubical approximation for the arm and wrist segments, the final representation of the path is simplified to three rectangular shapes with four tissue layers of specific thicknesses. The next step is to analyze the path to estimate its channel gain based on the dielectric properties and dimensions of the tissue layers.

This article has been accepted for publication in a future issue of this journal, but has not been fully edited. Content may change prior to final publication. Citation information: DOI 10.1109/TWC.2019.2921964, IEEE Transactions on Wireless Communications

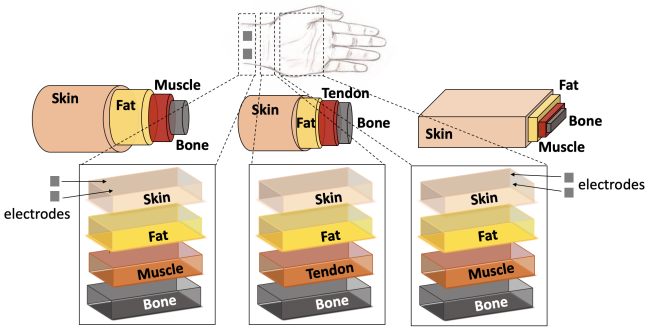

Fig. 2: Cubical approximation of arm, wrist and palm parts, and location of electrode attachments for galvanic coupling

A. *Tissue Equivalent Circuit*

GC requires two transmitting and two receiving electrodes attached on the skin. Thus, we formulate a tissue equivalent circuit (TEC) model to estimate the channel gain of the path between the arm and the palm. The impedance between two nodes of the TEC is calculated using an RC-circuit equivalent expression of the given path. The resistance and capacitance values of each path are calculated as $R = \frac{\rho L}{A_c}$ and $C = \frac{\epsilon A}{D}$.

The resistivity (ρ) and permittivity (ϵ) values for each tissue layer are frequency dependent and obtained from a published, standardized database [19]. Here, L represents the length of the path between the two nodes, A_c gives the cross-sectional area of the path, A is the surface area of the capacitance measured and D is the depth of the tissue. After calculating the resistance and capacitance of the path between two nodes, the impedance of the specific path is calculated using $Z = R + \frac{1}{C\omega j}$.

The impedance, resistivity, permittivity, length, cross-sectional area, surface area and thickness values are inputs to the model that we formulate next. The TEC for the entire path requires the calculation of five impedance values: Z_L (longitudinal), Z_D (inter-electrode), Z_C (cross) and Z_t (transverse), trivially obtained by replacing the respective ρ, ϵ, L and A values depending on the geometry of the path and using the above standard equations. The topview of the TEC is shown in Figure 3. The transverse impedance Z_t is between each layer and its adjacent one. A 3D representation of the TEC including the Z_t is depicted in Figure 4. The nodes are shown via capitalized letters; the arm-wrist and wrist-palm junctions share nodes. Hence, the Z_D and Z_t values are calculated by adding the two inverse impedances of the specific paths, as these

This article has been accepted for publication in a future issue of this journal, but has not been fully edited. Content may change prior to final publication. Citation information: DOI 10.1109/TWC.2019.2921964, IEEE Transactions on Wireless Communications

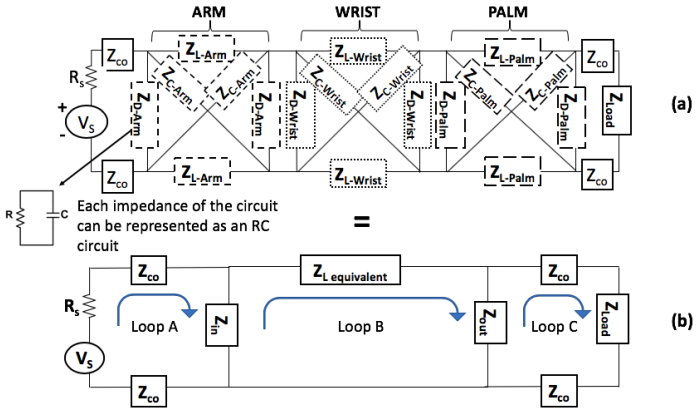

Fig. 3: Circuit (a) is the TEC of the skin layer in 2D. (b) is the equivalent of (a) used for channel gain calculations

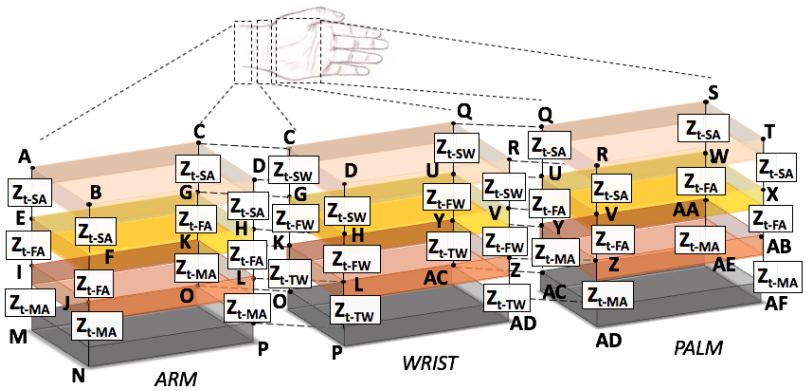

Fig. 4: 3D tissue equivalent circuit with transverse impedances for arm-wrist-palm path. The labeling of transverse impedances is Z_{t-ij}, for i $\in$ [S, F, M, T, B] corresponding to skin, fat, muscle, tendon, bone and j $\in$ [A, W, P] for arm, wrist, palm

impedances are parallel to each other, as also seen in the top-view of Figure 3.

We perform a nodal analysis using Kirchoff's Current Law (KCL) with the impedance of all paths to obtain an admittance matrix for the entire four-layer, thirty-two node equivalent circuit. For a sample node A, the nodal equation is:

$$I = \frac{V_A - V_B}{Z_D} + \frac{V_A - V_C}{Z_L} + \frac{V_A - V_D}{Z_C} + \frac{V_A - V_E}{Z_t} \tag{1}$$

Similarly, the equations for all nodes were derived, but not repeated here for space conservation. A simplified representation of the 32 KCL equations is the admittance matrix (A) of the 4-layer 3D circuit in equation (1).

This article has been accepted for publication in a future issue of this journal, but has not been fully edited. Content may change prior to final publication. Citation information: DOI 10.1109/TWC.2019.2921964, IEEE Transactions on Wireless Communications

$$A = \begin{bmatrix} \sum_{i\in C,L,D,t} \frac{1}{Z_{iSA}} & -\frac{1}{Z_{Dsa}} & -\frac{1}{Z_{Lsa}} & \dots & \dots & \dots & \dots & 0 \\ -\frac{1}{Z_{Dsa}} & \sum_{i\in C,L,D,t} \frac{1}{Z_{iSA}} & -\frac{1}{Z_{Csa}} & -\frac{1}{Z_{Lsa}} & 0 & -\frac{1}{Z_{tsa}} & \dots & 0 \\ \ddots & \ddots & \ddots & \ddots & \ddots & \ddots & \ddots & \ddots \\ 0 & \dots & \dots & \dots & -\frac{1}{Z_{Tmp}} & -\frac{1}{Z_{Cbp}} & -\frac{1}{Z_{Lbp}} & -\frac{1}{Z_{Dbp}} \end{bmatrix} \quad (2)$$

To obtain the gain of the TEC if a voltage is applied at the input terminals, an equivalent Pi-network is derived (Figure 3 (b)). The purpose of this step is to analyze the TEC as a two-port network with Z-parameters for the gain calculation. The Z-parameters of the circuit in Figure 3 (b) are calculated with Equations (3) - (6) which were derived from a 3-loop mesh analysis (loops A, B and C in Figure 3(b)), adhering to the two-port network parameter definitions.

$$z_{11} = R_s + 2Z_{co} + \frac{Z_{in}(Z_{Leq} + Z_{out})}{Z_{Leq} + Z_{in} + Z_{out}} \quad (3)$$

$$z_{21} = \frac{Z_{in}Z_{out}}{Z_{Leq} + Z_{in} + Z_{out}} \quad (4)$$

$$z_{12} = -\frac{Z_{in}Z_{out}}{Z_{Leq} + Z_{in} + Z_{out}} \quad (5)$$

$$z_{22} = 2Z_{co} + \frac{Z_{out}(Z_{Leq} + Z_{in})}{Z_{Leq} + Z_{in} + Z_{out}} \quad (6)$$

For example, Equation (3) calculates the z_{11} parameter (expressed as a ratio of the input voltage over the input current), by setting the current in Loop C equal to zero. The expressions for input voltage and current are subsequently derived from the resulting 2-loop circuit (loops A and B).

In summary, our model takes as input the length of the arm, wrist and palm, the size and distance between transmitting and receiving electrodes as well as the signal frequency. The admittance matrix is then constructed using the equations and inputs of the model. The gain of the entire arm-wrist-palm path is then calculated as the logarithmic ratio of the impedance over the output (between nodes S and T) and that of the input (between nodes A and B). The gain of the channel can be investigated using the model under several configurations and plays an important role in the design parameters of the GC communication system. The 3D arm-wrist-palm model is validated experimentally, in the next subsection, for various scenarios. Subsequently, we utilize the knowledge of the channel response to test and compare various aspects of the

This article has been accepted for publication in a future issue of this journal, but has not been fully edited. Content may change prior to final publication. Citation information: DOI 10.1109/TWC.2019.2921964, IEEE Transactions on Wireless Communications

GC communication system design in MATLAB, before we demonstrate the implementation of a real system.

B. Experimental Model Validation

The proposed model is used to obtain (i) distances at which the gain of the channel is high (as we shall show later, the gain shows non-uniform behavior), and (ii) to set the frequency of operation and inter-electrode distance. For these reasons, we first validate the arm-wrist-palm model through an experimental setup. We conduct experiments on an electrically equivalent synthetic tissue phantom from Syndaver Labs^{TM} that represents the human arm, wrist and palm components. For all reported experimental results, the gain between different parts of the phantom is calculated by measuring the input and output Peak-to-Peak voltage of a sinusoid at various distances. The Analog Discovery ^{TM} module is used as both a waveform generator and oscilloscope to transmit a sinusoid and read the signal at different parts of the phantom, respectively. To avoid the use of a common ground between input and output, two Analog Discovery devices are employed, each with its own PC connection. Balun circuits (Schaffner IT239) bridge the connection between the phantom and the Analog Discoveries. This aids in additional isolation of the common ground return path that can be caused by the lack of EMI shielding and large base of the laptops (transmitter and receiver) attached to the same surface. The skin-to-skin channel gain is important as it is the main propagation path of the smart-device. Therefore, to ensure optimal contact in the setup, the wires of the oscilloscope measuring voltage as well as the function generator are minimally inserted into the skin layer, without penetrating the subsequent tissue layers of the phantom. We model the edge of the wires that are attached on the skin as electrodes with <1 mm^2 surface area to accurately represent the experimental configuration [17].

Figure 5a depicts the results of the model validation. Both the experimental setup and our model maximize the gain between 200 and 500 KHz. The gain over a 10 cm distance are overall higher than those for 15 cm, as expected, and match the trends associated with the model predictions for all frequencies. The varying hydration levels of skin layer measurements, shown in [1], support the claim that a deviation between model and experimental data of 5 dB or less provides suitable results. Henceforth, we specifically focus on the gain prediction at around 10 cm distance, which is most relevant to our biometric-based secure communication.

This article has been accepted for publication in a future issue of this journal, but has not been fully edited. Content may change prior to final publication. Citation information: DOI 10.1109/TWC.2019.2921964, IEEE Transactions on Wireless Communications

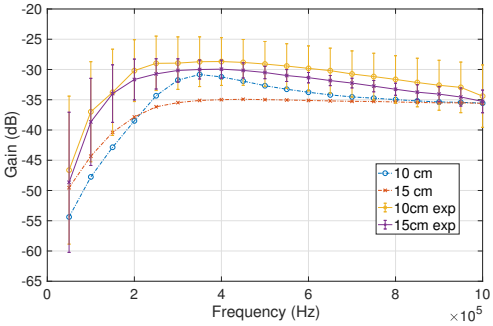

(a) Experimental and model data comparison for gain vs. frequency

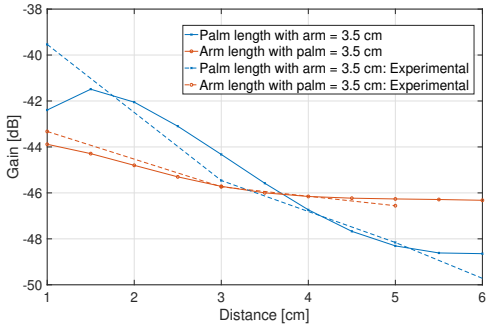

(b) Experimental and model data comparison for gain vs. distance, varying palm length (f_c = 400 kHz)

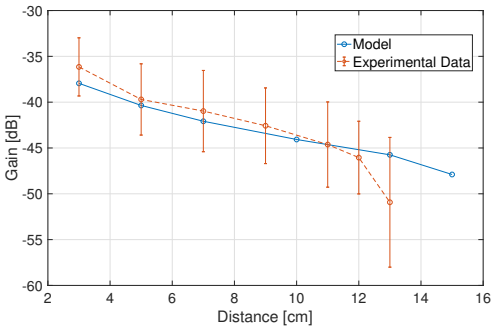

(c) Experimental and model data comparison for gain vs. distance (f_c = 400 kHz)

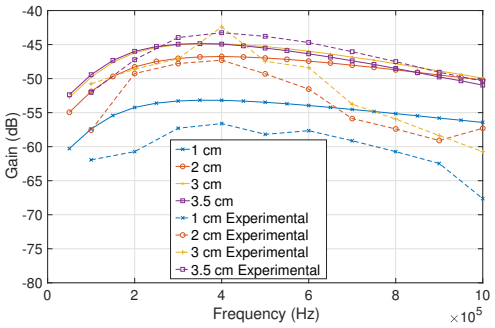

(d) Experimental and model data comparison of gain vs. frequency for varying electrode separation distances

Fig. 5: 3D tissue equivalent model validation

Noting the frequency range where the gain is the highest, we conducted a series of experiments with varying distances between the palm and the arm, to test the reliability of the model as the input parameter of distance changes. This captures possible relative positions of the wristband and the mobile device. Figure 5b shows the gain of a sinusoidal input operating at 400 kHz over various distances by altering the palm and arm lengths. We draw two conclusions from the results: the model closely predicts the gain with varying distances, though varying the length of the palm portion of the path leads to increasing variation in gain than the arm portion. A possible explanation of this phenomenon is the increased thickness of the palm skin layer. Since the gain is calculated on the skin layer, the thickness of the skin affects the gain to a significant extent. When we vary the arm and palm distances around the wrist, we see that the predicted

This article has been accepted for publication in a future issue of this journal, but has not been fully edited. Content may change prior to final publication. Citation information: DOI 10.1109/TWC.2019.2921964, IEEE Transactions on Wireless Communications

versus observed gain values lie within an acceptable experimental margin of error (Figure 5c). As expected, the gain is highest for shorter distances between transmitter and receiver.

Finally, we study the impact of the inter-electrode separation for the two GC transmitting and receiving electrodes. Results indicate that greater inter-electrode distance between the individual pairs of the transmitting and receiving electrodes leads to a higher gain between the transmitter-receiver nodes, when all other parameters remain constant. Greater inter-electrode distance in galvanic coupling leads to a higher potential between the two electrodes, and therefore, a higher gain between transmitter and receiver. Similar to the previous experiments, the model predictions match closely with the experimental results, proving once again that the arm-wrist-palm model can predict the channel behavior with high accuracy (Figure 5d).

With the theoretical model validated, we focus next on the communication system and its prototype design.

TABLE I: Tissue thickness values (mm)

	Skin	Fat	Muscle	Tendon	Bone
Arm	1.00	7.00	15.00	-	20.00
Wrist	1.00	7.00	-	1.50	15.30
Palm	1.40	7.00	9.00 [20]	-	9.17 [21]

III. Choice of GC modulation scheme

The GC channel model, proposed in Section II-A and experimentally validated in Section II-B, is the starting point of our communication system design. We employ the use of the analytical channel model to store the channel frequency response for reproducible simulations. We then create multiple realizations of the channel behavior by flexibly controlling the center frequency, inter-electrode separation and the amount of arm and palm channel lengths to find the transmitter and receiver link configurations that yield the highest gain values. We select the best combinatorial approach from these parameters and formulate a channel frequency response to test multiple candidate narrow-band modulation schemes with various transmission bandwidths (those that yield flat fading characteristics) using MATLAB. Since we have a tighter constraint on power consumption as opposed to available bandwidth, non-coherent systems and/or techniques with lower modulation orders are more suited for our application. Our goal is to achieve a target BER

This article has been accepted for publication in a future issue of this journal, but has not been fully edited. Content may change prior to final publication. Citation information: DOI 10.1109/TWC.2019.2921964, IEEE Transactions on Wireless Communications

TABLE II: GC-IBC PHY layer performance comparison

System	Occupied Bandwidth	Min. Tx Power	Max Bit rate	Energy Consumption	Modulation Order
BFSK	209.5 kHz	-8 dBm	50 kbps	590.5 μJ	2
BPSK	52.3 kHz	-13 dBm	50 kbps	2.75 mJ	2
OOK	52.57 kHz	-9 dBm	50 kbps	158.2 μJ	2

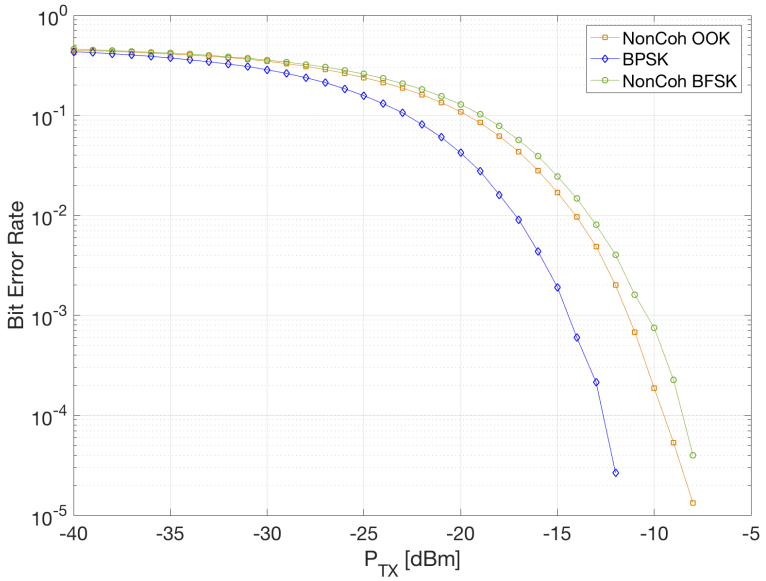

Fig. 6: BER vs trasnmit power for various modulation schemes

of 10^{-4} or better by selecting one of: Binary Frequency Shift Keying (BFSK), On-Off Keying (OOK) and Binary Phase Shift Keying (BPSK).

A. Power Consumption Analysis

In order to investigate the power consumption of each system, we model the power required for all analog front-end components depicted in the aforementioned modulation schemes in the MATLAB environment. This model is based on [22], where equations for calculating the power consumption of ASIC implementations are presented. Here, the signal bandwidth, peak-to-average-power ratio (PAPR), modulation order, and channel gain at various frequencies have an affect on the performance. The overall energy consumption of a system, which depends on its front-end components, is calculated in [22] with Equation (7).

This article has been accepted for publication in a future issue of this journal, but has not been fully edited. Content may change prior to final publication. Citation information: DOI 10.1109/TWC.2019.2921964, IEEE Transactions on Wireless Communications

$$E_c = ((P_{Tx} + P_{out}) \cdot T_{on}) + (P_{Rx} \cdot R_{on}) \tag{7}$$

The variables P_{Tx} and P_{Rx} represent the total power consumption from the transmitter and receiver electronics, respectively. These values are obtained from the sum of the contribution from the individual components of each system design, which consist of a variation of one or more of analog front-end devices modeled above. The output power (P_{out}) required for the desired level of link reliability is obtained from the data presented in Figure 6. The factors of T_{on} and R_{on}, represent the time that the transmitter and receiver elements are active, respectively and are derived from packet size and data rate. The front-end components of the design are based on the modulation schemes investigated in this section can be found in Table III. The hardware components are simulated with their respective systems for the purpose of calculating the BER and energy consumption of each modulation scheme.

TABLE III: Front-end components for system design with BPSK, OOK and BFSK modulation

Modulation	Transmitter	Receiver
BPSK	DAC, mix, VCO, PA	ADC, PLL, mix, VCO, filter
OOK	DAC, mix, VCO, PA	ADC, filter
BFSK	DAC, 2 mix, 2 VCO, PA	ADC, 2 filters

The transmitted and received power of a system designed to perform BFSK modulation is calculated as follows:

$$P_{Tx_{BFSK}} = P_{DAC} + 2(P_{mix} + P_{VCO}) + P_{PA} \tag{8}$$

$$P_{Rx_{BFSK}} = P_{ADC} + 2P_{filter} \tag{9}$$

The power of each component is calculated using equations from [22]. These are defined as P_{PA}, P_{mix}, P_{filter}, P_{DAC}, P_{ADC}, P_{PLL} and P_{VCO} and represent the power consumption for the power amplifier (PA), the mixer, the analog filter, the digital to analog converter (DAC), analog to digital converter (ADC), phase locked loop (PLL) and the voltage controlled oscillator (VCO), respectively. We use the operating characteristics of the Teensy MCU, specified in the data sheet, to set parameters of the components utilized in eventual system design in Section IV such as the supply voltage, ADC clock frequency and VCO operating frequency.

Similarly, with the components listed in Table III and equations (8)-(9), the transmitted and received powers for all modulation schemes are calculated. The energy consumption of the entire

system for the three candidate modulation schemes is also calculated and represented in Table II using Equation (7).

B. Performance Comparison

Constrained by the physical limitations of the synthetic tissue phantom that is used for empirical validation and the optimal center-frequency gain, we select the channel response generated from the following parameters to compare various systems in the MATLAB environment: a center frequency of 400 kHz, an inter-electrode separation distance of 3 cm, and a total channel length of 10 cm. Figure 6 plots BER versus transmit power (an important limiting factor when considering GC communication within the body). The minimum transmit power needed to obtain the target BER for each modulation scheme is listed in Table II. To fairly compare each technique, the symbol rate is fixed to a value of 50 kbps. Results indicate that the BPSK system offers an improvement in terms of power efficiency and a gradual improvement in terms of bandwidth efficiency, as it is able to achieve the same target BER while occupying less spectrum, and transmitting with less power. However, the performance increase is approximately 3dB when compared to the modulation techniques of OOK and BFSK. At the same time, it can be seen that the energy consumption of BPSK is approximately 18x of the OOK for the GC channel (Table II). These results indicate that the marginal increase in BER performance does not justify the need to increase system complexity, hardware footprint and energy consumption for a low-power wearable. Based on these characteristics, we determine that OOK modulation is better suited at the PHY layer for integration into an embedded system platform for simple biometric signal like ECG transmission via GC.

IV. Galvanic Coupling System Design

Our prototype system consists of a Teensy microcontroller unit (MCU) with supporting analog front-end hardware for signal modulation and detection. At the fundamental level, the components within the system have the flexibility to implement either of the modulation schemes discussed in Section III.

A. System Overview

Figure 7a illustrates our design and implementation of a complete system that securely transmits biometric data. The transmitter MCU is configured to transmit with a biometric signature

This article has been accepted for publication in a future issue of this journal, but has not been fully edited. Content may change prior to final publication. Citation information: DOI 10.1109/TWC.2019.2921964, IEEE Transactions on Wireless Communications

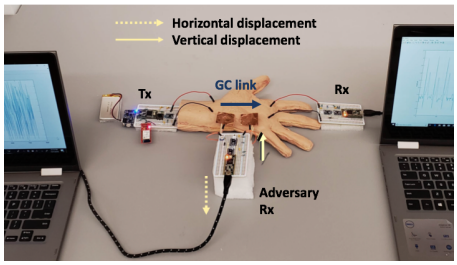

(a)

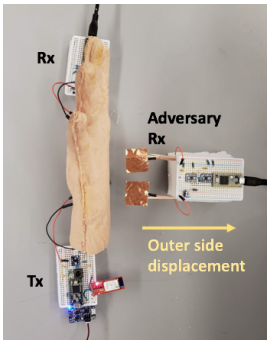

(b)

Fig. 7: Physical GC communication system testbed

unique to the individual (in our scenario, the ECG signal). To prepare for signal transmission, the pulse width modulation (PWM) output of the Teensy-Tx, combined with controllable internal logic, is toggled based on the binary data and pre-selected bit duration. A low pass filter removes the signal harmonics in the frequency domain, while preserving the center tone ($f_c = 100kHz$). This center frequency is chosen, despite the knowledge of an operating frequency that can yield higher channel gain, due to the gain bandwidth product limitation of the operational amplifier used in receiving chain. The remainder of the parameters utilized in the MATLAB simulation are translated over to the physical domain, and are thus represented in the prototype testbed setup.

The data is sent through the tissue wireless channel within the payload of a frame, which consists of a preamble (13-bit Barker code) for synchronization, data length field (8 bits), payload (64 bits) and an 8-bit CRC. Once the signal propagates through the human body channel, the analog front-end receiver hardware utilizes a high pass filter (HPF) to remove any low-frequency noise associated with power-line interference and/or baseline drift. The receiver amplifier (MAX4488 by Maxim Integrated^{TM}) counteracts the attenuation of the channel and high pass filter, while raising the signal level to meet the turn-on voltage requirements of the schottky

This article has been accepted for publication in a future issue of this journal, but has not been fully edited. Content may change prior to final publication. Citation information: DOI 10.1109/TWC.2019.2921964, IEEE Transactions on Wireless Communications

Fig. 8: Transmitted and reproduced signal in time and frequency domain

diode (used in the subsequent system block). Next, we employ an envelope detector circuit to convert the signal back to baseband and to remove any possible carrier wave oscillations that could have an adverse affect on the input to the comparator (MAX4488) trigger at the final stage. The comparator threshold is dynamically controlled through a potentiometer, and it is designed to reproduce the original binary bit sequence delivered from the transmitter. Data packets are detected by the Teensy-Rx, decoded and forwarded through the serial port to MATLAB for subsequent processing.

B. System Performance

•**Hardware Validation:** The transmitter and receiver performance is illustrated through the output of an Analog Discovery module. The OOK pulse and its corresponding center tone are generated at the transmitter end. Figure 8 portrays the transmitter and receiver performance in both the time (top) and frequency (bottom) domain. The latter provides validation of the comparator output, returning the original bit sequence that is fed into the ADC of the Teensy-Rx. The former depicts the transmitted signal output. The time domain plots indicate the equivalent bit duration of the two signals, and the frequency domain plots indicate the appropriate operating frequency and that the received signal has been translated from passband to baseband.

•**Power Consumption:** We determine the current and subsequently the power consumed by the transmitting and receiving hardware using the shunt resistor method. We leverage high-side insertion, or placing the 1Ω shunt between the positive supply and the load, in order avoid potential ground loops. For our setup, we used the adafruit PowerBoost 1000C circuit with a 3.7V rechargeable battery to power the Teensy, which then delivers 3.3 V of power to the remaining Tx and Rx circuitry.

We use the Analog Discovery module to measure the voltage drop across the shunt resistor and employ it's hardware support package with MATLAB to export the data into a host PC for

This article has been accepted for publication in a future issue of this journal, but has not been fully edited. Content may change prior to final publication. Citation information: DOI 10.1109/TWC.2019.2921964, IEEE Transactions on Wireless Communications

TABLE IV: Average current and power consumption for Teensy Tx and Rx

Mode	Current	Power
Tx Idle	938.87 μA	3.098 mW
Rx Idle	3.29 mA	10.87 mW
Rx Listen	14.307 mA	47.20 mW
Tx On	39.77 mA	131.25 mW
Rx On	17.32 mA	57.15 mW

processing. We then calculate the current consumed by using the relationship between resistance and voltage in Ohm's law ($V = IR$). We subsequently calculate the power consumption by multiplying the current drawn by the supply voltage ($P = VI$). For the transmitting Teensy, we consider the transition between an idle mode and a mode in which the Tx is on and actively sending modulated bits. At the receiver, we account for a transition between an idle mode, an Rx listening mode and an Rx on (receiving) mode. During the idle modes, the MCU is placed in a deep sleep state, via software, where most peripherals are completely shut off. In the Rx listening mode and Rx on modes, we achieve additional energy saving by placing the MCU in a low power state where the peripheral clocks run at a lower speed.

During the operations in which the system is not transmitting or receiving, the operational amplifiers used within the Tx and Rx chain are in shutdown mode and consume approximately $.01\mu A$. In the active states of transmission and reception, the operational amplifiers draw 2.2 mA of current. Table IV presents the current and power consumption for all of the aforementioned modes for the transmitter and receiver, with the inclusion of their accompanying front-end hardware. We observe that the transmitting mode consumes the most power, followed by the receiving mode. This behavior is caused by the inability of the Tx-Teensy to initialize the necessary transmitting functions in a low power state and thus, the normal operating mode must be used. Figures 9a and 9b illustrate the total measured current drawn by Teensy Tx and Rx, plotted against time, for different modes of operation. Using the relationship between, power and time, ($E_c = [P_{Tx} \cdot T_{TXon}] + [P_{Rx} \cdot T_{RXon}]$), we determine that the total average energy consumption of the Tx and Rx are 523.95 mJ and 565.07 mJ, respectively. When comparing the simulated energy consumption results for OOK modulation, presented in Section III, there exists a significant performance difference. In order to more accurately compare these two energy

This article has been accepted for publication in a future issue of this journal, but has not been fully edited. Content may change prior to final publication. Citation information: DOI 10.1109/TWC.2019.2921964, IEEE Transactions on Wireless Communications

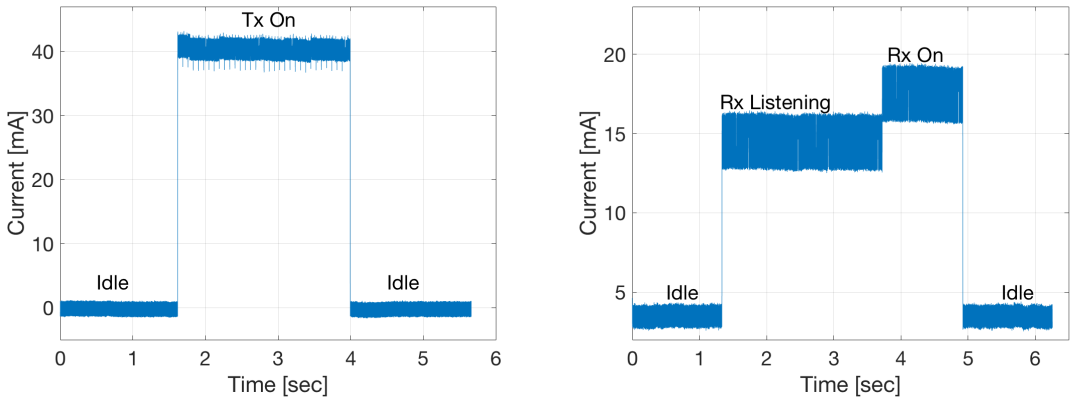

(a) (b)

Fig. 9: Measured current draw by Tx (a) and Rx (b) Teensy

consumption numbers, it is best to implement the system on an application-specific integrated circuit (ASIC) and apply industry caliber research and development for ideal power savings to be achieved [23].

•**Energy Per Bit:** We define the energy per bit as the ratio of the amount of energy delivered into the synthetic tissue medium over the total amount of bits sent through that same medium. We derive its value from the energy consumption values of the transmitter, while in an active state, over the total amount of bits used to transmit one sample ECG recording. Using this description, we measure the energy per bit to be approximately 51 μJ/bit. For an RF-intra-body communication link presented in [24], whose signals still substantially leak into the area surrounding the human body, an energy efficiency of 2.90 nJ/bit is achieved. The difference in performance can be attributed to the RF case employing an ASIC implementation, while our design, which is built from COTS device is not optimized for low power operation.

•**Bit Error Rate:** We tested the end-to-end link performance by using actual ECG signal traces. Figure 10 depicts the BER for various transmit powers for a link distance of 10 cm. The transmit power is calculated by measuring the impedance of the synthetic tissue phantom across the input terminals of the transmit electrodes, and using the equation $P_{Tx} = V^2/R$. To alter the transmit power levels, we vary the output voltage through the use of a basic attenuator circuit. Observations indicate the experimental capability of achieving a BER of 10^{-6} for a transmit power of -2 dBm (0 BER for simulated trials) and no errors for a transmit power of 0 dBm for both experimental and simulated tests. Longer distances can be supported, at the expense of

This article has been accepted for publication in a future issue of this journal, but has not been fully edited. Content may change prior to final publication. Citation information: DOI 10.1109/TWC.2019.2921964, IEEE Transactions on Wireless Communications

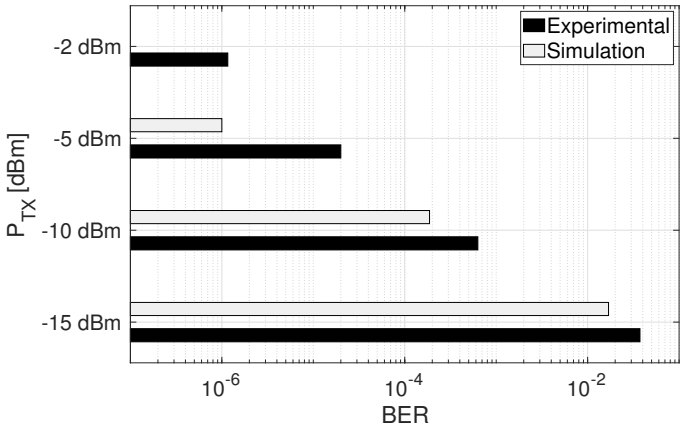

Fig. 10: BER vs transmit power for GC-transceiver OOK modulation

higher BER and consequently, higher transmit power, or by introducing forward error correction code.

V. Eavesdropping Susceptibility

To substantiate the claims of a secure biometric transmission system with minimal signal leakage outside the body, we experimentally confirm the level of received signal strength that may be overheard by an over-the-air entity and one that comes in direct contact with the human body medium.

A. Over-the-Air Signal Susceptibility

We evaluate the over-the-air signal susceptibility of our system against the work conducted in [13]-[16], which leverage the use of capacitive coupling (CC) and apply the work in [25] to motivate the use of a hybrid coupling method (GC configuration at the transmitter and CC configuration at the receiver). The purpose of this comparison is to evaluate the susceptibility of our design to over-the-air (OTA) sniffing against the most commonly used non-RF intra-body communication methods in wearables. We perform a series of experiments where we measure the received signal strength (RSS) and BER of an adversarial receiver with the adequate hardware and software means to attempt signal interception. Thus, the malicious receiver is designed as an exact replica of the receiver presented in Section IV only it does not come in physical contact with the phantom. The adversary also consists of two copper electrodes measuring at 3x3 cm with an electrode separation of 5 cm when configured for GC. The RSS and BER are measured at various arrangements representing distances (as shown in Figure 7a and 7b) displaced horizontally (with

This article has been accepted for publication in a future issue of this journal, but has not been fully edited. Content may change prior to final publication. Citation information: DOI 10.1109/TWC.2019.2921964, IEEE Transactions on Wireless Communications

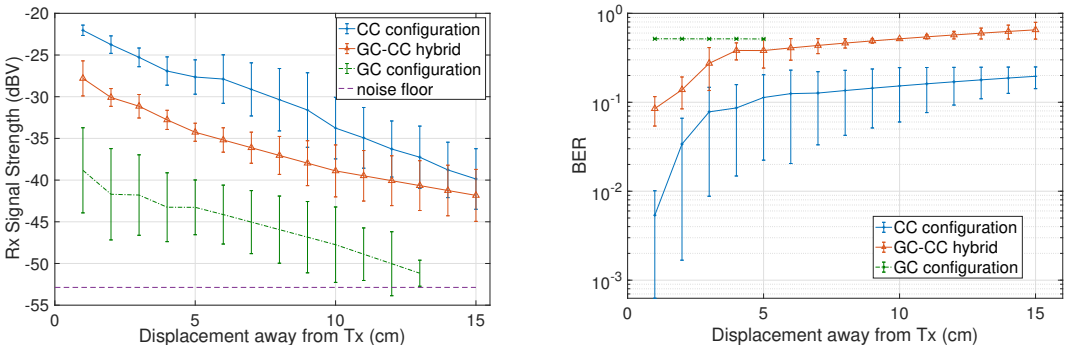

(a) (b)

Fig. 11: Average RSS (a) and BER (b) at over-the-air adversary Rx at various distances from Tx

the palm facing up), vertically and on the outer part of the phantom arm, opposite the side of the tissue where the true receiver is located. Results from Figure 11a illustrate that the RSS at the adversary receiver decreases as we move away from the transmitter in any direction. For all three displacement orientations, the signal strength at the adversary Rx is lowest for the GC method, followed by the hybrid method and then lastly, the CC method. This behavior can be explained from [25] as the hybrid method forms a return path through the environment (as in the CC case) but its range is confined to a portion of the body, that in which the transmitter is located, as opposed to the entire body. Ultimately, these results show the use of GC to transmit a signal in the body provides a more secure channel where the average RSS at the adversary Rx is at the noise floor at a distance of 13 cm, making decoding very difficult. To confirm the level of decoding at the adversary Rx, we conduct the second set of experiments to measure the adversary BER at different positions around the phantom, identical to those in the RSS studies. The results of Figure 11b indicate that the adversarial Rx with GC configuration does not have the capability to decode the signal at any distance or orientation. The CC configuration, however, allows for significantly lower BER values in distances up to 15 centimeters with nearly a 10^{-4} BER at distance of 1 cm away from the tissue, which can lead to a sniffing attack. We thereby conclude that the choice of GC as the method of intra-body communication for our system is advantageous in establishing a secure channel to transmit biometric data.

This article has been accepted for publication in a future issue of this journal, but has not been fully edited. Content may change prior to final publication. Citation information: DOI 10.1109/TWC.2019.2921964, IEEE Transactions on Wireless Communications

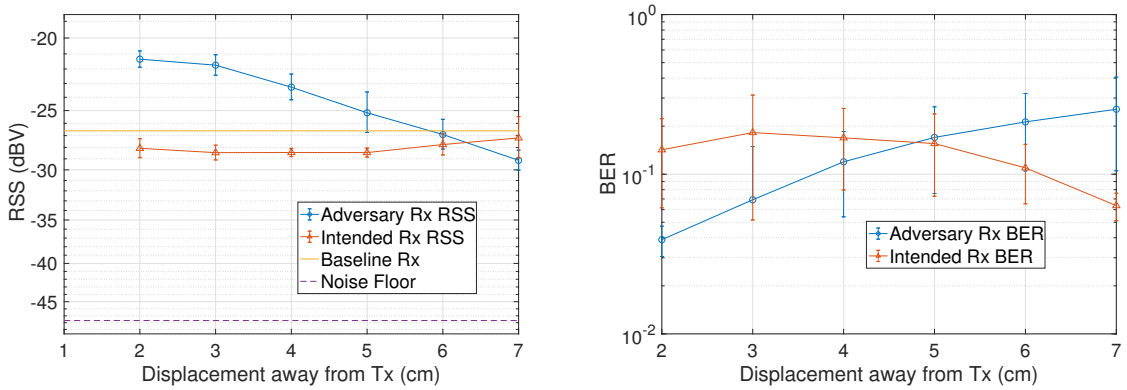

(a) (b)

Fig. 12: Average RSS (a) and BER (b) at contact adversary Rx at various distances from Tx

B. Contact-based Susceptibility

We evaluate the impact of an adversarial receiver that lies in direct contact with the human body, during data transmission, at various places throughout the channel. We utilize a synthetic tissue slab (also provided by Syndaver Labs) to act as the medium in which the transmitter and intended receiver operate. The adversarial receiver, whose system design is an exact replica of the intended receiver, takes the form of the synthetic tissue hand that we have utilized in all testbed experiments conducted thus far. The electrode placement options include fingertip, palm and wrist electrode positioning. However, prior experimental work indicated that the fingertip method of electrode placement yielded the highest results in terms of received signal strength. Thus, we connect both the signal and ground electrodes on the fingertips of the index and middle finger, with an electrode separation of 4 cm. We place the adversarial receiver in contact with synthetic tissue slab at positions (shown in Figure 13) dubbed *inside line-of-sight* (iLOS) and *reverse line-of-sight* (rLOS), and measure the RSS and BER over distances displaced from the location of the Tx. Figure 12a and 12b depict the RSS and BER plots versus displaced distance from the transmitter, respectively. Here we observe that the adversarial Rx can still obtain a BER of $> 10^{-2}$, up to 7 centimeters away from the transmitter. The values observed in this experiment are higher than those seen in the OTA test, as we expect. However, the adversarial receiver does not obtain a significant advantage in choosing to intercept data using one method versus the other. The results shown in Figure 12a and 12b also reveal that when there is contact on the channel of interest, the intended receiver also suffers a loss in RSS and increase in BER

This article has been accepted for publication in a future issue of this journal, but has not been fully edited. Content may change prior to final publication. Citation information: DOI 10.1109/TWC.2019.2921964, IEEE Transactions on Wireless Communications

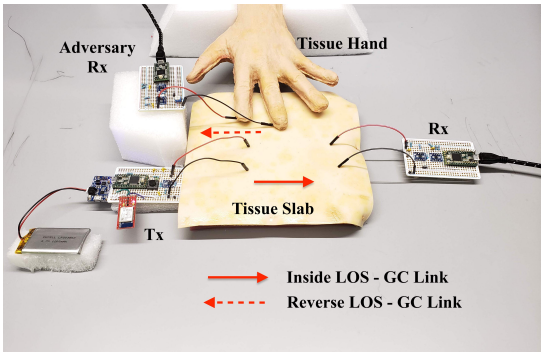

Fig. 13: GC Communication testbed for contact-based experiments

(as opposed to the OTA case). As the adversarial Rx moves further away from the Tx, the RSS of the intended Rx begins to improve, subsequently causing a decrease in BER. However, this performance when compared to the case when there is no contact with the channel is still significantly degraded. These experiments indicate that the presence of human body contact (whether accidental or intentional), in close proximity to the Tx and intended Rx during any part of the data transmission process, can cause erroneous results. To further understand this behavior, we perform channel sounding experiments in a similar manner to [26], in the subsequent section, to gain a better understanding of what phenomenon is occurring at the channel level.

VI. Detection of Adverse Channel Conditions

In this section, we present findings that provide a categorization of the channel behavior observed when direct contact is made during the data transmission and reception process. We also present a means of detecting and mitigating the effects of direct contact by providing alternative transmission parameters for the sending and receiving of biophysical data.

A. Impact of Channel Contact

We design and implement a correlative channel sounder in order to measure and and record (for post processing) the channel impulse and frequency response of the tissue slab channel in situations where there is no contact and direct contact. This method of channel modeling is based on the observed behavior when applying a white noise signal to the input of a linear system. The output of such a system is cross-correlated with a delayed replica of the input producing a scaled version of the system impulse response. However, in practice the goal is

This article has been accepted for publication in a future issue of this journal, but has not been fully edited. Content may change prior to final publication. Citation information: DOI 10.1109/TWC.2019.2921964, IEEE Transactions on Wireless Communications

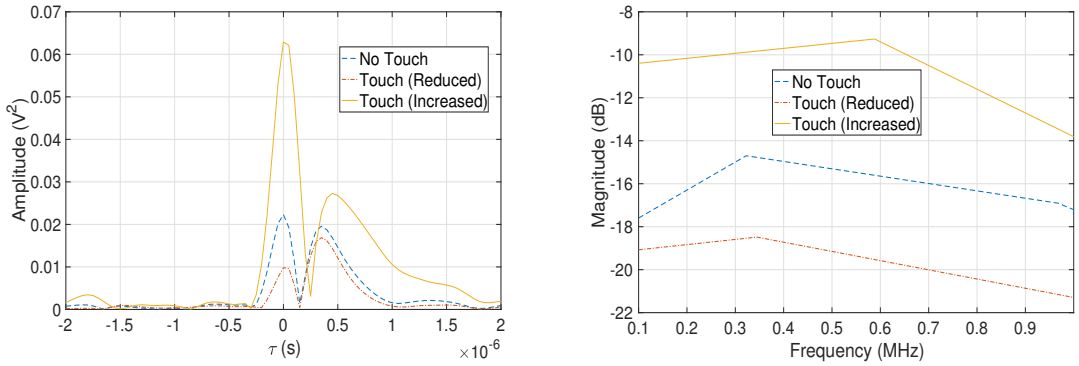

(a) (b)

Fig. 14: Channel impulse (a) and frequency response (b) for different contact scenarios

to leverage a deterministic waveform that resembles noise-like characteristics. [27]. Therefore, we design a maximum length Pseudorandom Noise (PN) sequence using a linear-feedback shift register (with $2^m - 1$ cyclic shifts and $m = 14$) to modulate and send through the channel. We specifically employ single-carrier BPSK modulation ($f_c = 550kHz$) on this PN-sequence with a chip duration of 250 nanoseconds, which equates to approximately 4 MHz of bandwidth. We adhere to the general design criteria of the PN-sequences for channel sounding, which prefers a signal that yield an auto-correlation function with a high correlation peak at the zero-shift point and produce a high peak-to-off-peak ratio. We selected the signal bandwidth to ensure we could resolve any possible multi-path components while adhering to the frequency range of our GC channel (100 kHz to 1 MHz).

We perform channel sounding measurements for three specific cases that relate to scenarios of no contact and channel contact. The baseline case, or case 1, we take measurements when no external contact is made with the channel, while maintaining the same link distance and electrode separation. For cases 2 and 3 we repeat the same measurement setup but with external contact that causes a visible increase and decrease in the RSS, respectively. Using a similar testbed setup to what is depicted in Figure 13, we replace the custom Tx and Rx hardware each with an Analog Discovery module. The PN-sequence was designed in the MATLAB environment, exported to the `.csv` file format, and loaded into the signal generation software on the Analog Discovery. At the receiver side, we use the oscilloscope feature of the Analog Discovery to export the data into MATLAB for the generation of the channel impulse response and channel frequency response.

This article has been accepted for publication in a future issue of this journal, but has not been fully edited. Content may change prior to final publication. Citation information: DOI 10.1109/TWC.2019.2921964, IEEE Transactions on Wireless Communications

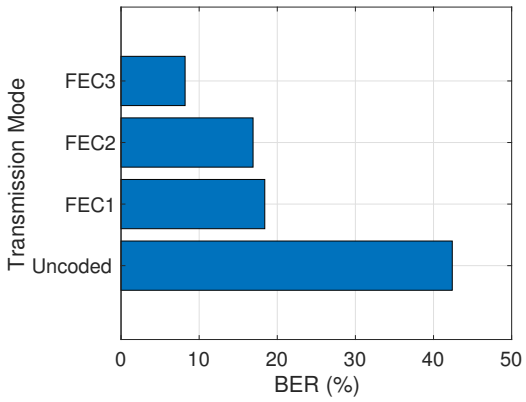

Fig. 15: FEC performance during contact-induced channel experiments

Figure 14a depicts the channel impulse response for all three cases, superimposed for visual purposes. Results for the baseline case present two multi-path components with almost equivalent amplitude. When examining the channel frequency response for the baseline case, the AWGN channel nature that is observed within the GC-research community is validated for our target range of transmission bandwidth (1 Khz to 50 Khz). However, we observe that the presence of touch changes the nature of the impulse response. For example, an external touch in a location that causes an increase in RSS (channel geometry dependent) alters the impulse response such that the first tap is greater in magnitude when compared to the second tap. The opposite case takes place in locations in which external contact decreases the RSS. These effects are also displayed in the channel frequency response presented in Figure 14b. For our maximum transmission bandwidth range, we still observe a relatively flat fading channel. However, the channel gain can increase or decrease based on location-dependent, external contact with the human body medium. These results validate the behavior observed at both the intended Rx and adversarial Rx that we present in our contact-based experiments within Section V. Regardless of the intention behind eliciting contact upon the human body medium, the intended receiver can still undergo periods of performance degradation. In order to account for such an occurrence, we design a system for detecting periods of channel contact that produce an abrupt change in received data quality. We also provide insight on the appropriate levels of forward error correction (FEC) codes to apply in order mitigate this drop off in performance. Both of these contributions are described in detail in the subsequent subsection.

B. FEC Selection for Adverse Channel Conditions

We experimentally induce contact-based events into the synthetic tissue medium, during data transmission, specifically focusing on improving the BER performance of the intended receiver. The preamble sequence, originally used solely for frame synchronization, is modified to encompass the PN-sequence used in the previous subsection. The inclusion of a CRC8 (located in the trailer) for error detection is used to track an instantaneous packet error in between correct frames. If this occurrence continues, the received preamble is cross-correlated with the original data sequence to obtain the channel impulse response and examine if a morphological change has occurred that indicates a touch. In our current system, we experimentally uncover what change in transmission parameters are necessary to combat the channel degradation brought on by touch. Thus, we evaluate the impact of various levels of FEC to determine what code rates are appropriate for this use case. We compare the performance of the system for uncoded transmission, and transmission with Hamming codes for rates of 1/3 and 4/7, notated as FEC1 and FEC2 respectively. As seen in figure 15, introducing the simplistic FEC1 scheme provides a large improvement to the average BER from approximately 43% to 18%. The adoption of FEC2 yields very little increase in the performance, resulting in a BER of approximately 17%. Thus, we included trials with a larger, more efficient Hamming code of (15,11), which we call FEC3. These results show a further reduction in BER, validating the need to incorporate adaptive transmission of multiple FEC schemes, for future system designs, where channel state feedback is provided by the receiver.

VII. Discussion and Conclusions

We developed a model of the tissue communication channel by using equivalent electrical circuits that matched closely with experimental testbed measurements. We identified OOK as the preferred modulation technique for our application, and developed a proof-of-concept testbed composed of an embedded system implementation with supporting hardware and a synthetic tissue phantom. The system functions reliably, transmitting a sample ECG signal over a 10 cm human tissue path with a transmit power of -2 dBm, while maintaining a BER of 10^{-6}. We demonstrated the GC-secure method of transmitting biometric information by measuring the level of over-the-air signal leakage from the vantage point of an adversarial receiver with satisfactory knowledge of our system design. We also presented the adversarial Rx advantage when in direct contact with the body medium, while providing a means to characterize and

mitigate the observed channel behavior by detecting the manifestation of any touch-based event. Our future approach will be focused on exploring the utility of ECG and other biological signals for the development of an end-to-end biometric authentication system and developing ways to transmit the GC-signal over longer distances. Furthermore, we will devise adaptive modulation schemes and reconfigurable front-ends that may adapt the link/physical layer operation based on changing authentication needs or wearable sensor data reporting rates.

APPENDIX A
ECG SIGNAL CLASSIFICATION CASE STUDY

We conduct a preliminary proof-of-concept study with ECG signals to demonstrate the possibility of recreating similar levels of ECG classification accuracy with those values reported in literature, albeit with the intention of implementing a much simpler algorithm. Within the MATLAB environment features are extracted from the signals provided from the ECD-ID Database by PhysioNet [18], which consists of measurements sampled at 500 Hz, taken over a 6 month period from 90 subjects in a Lead I configuration. The experimental setup for this portion of the study utilizes 20 subjects with 5 recordings each, for training and testing, evaluating them individually against all other subjects and recordings of each subject. An additional 67 subjects with 1 recording each are strictly used to test known instances of the opposing class.

In contrast to authentication methods that utilize a database to compare pre-existing biometric inputs from multiple subjects, this form of pattern recognition is designed to distinguish a particular class from all other possible inputs into the system (one vs. rest or one-class classification). This strategy solely necessitates learning from the class or person of interest and no information about the other classes are present. The basic approach involves producing a result that is a representation of a confidence score used in the decision making. Decision boundaries are formed around the class of interest, with the objective of accepting or rejecting the incoming data based on the measure of certainty. This method is chosen for the sake of resembling a suitable scenario for mobile device authentication, where typically only one user is registering for access.

•**One-Class Classification Performance:** Our one-class classifier (OCC) implementation consists of a simplified enrollment and authentication process. In the enrollment phase, we detect the QRS portion of an ECG signal (exemplified in Figure 16), separate the entire ECG recording into non-overlapping segments (one segment equals one PQRST portion) and averaging off all separated beats to form a template. During this enrollment phase, the segments of one recording

This article has been accepted for publication in a future issue of this journal, but has not been fully edited. Content may change prior to final publication. Citation information: DOI 10.1109/TWC.2019.2921964, IEEE Transactions on Wireless Communications

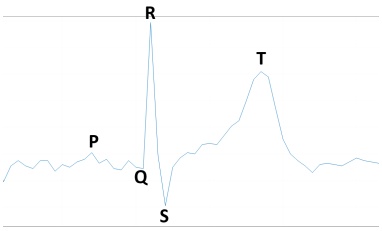

Fig. 16: Illustration of one ECG PQRST segment

		Classified	
		Not Sub. 1	Sub. 1
Actual	Not Sub. 1	3026	54
	Sub. 1	88	292
	Total Accuracy = 95.89 %		
	False Positive	0.0174	
	True Positive	0.768	

TABLE V: Confusion Matrix for One-Class Classification using 4 beats in the authentication

are cross-correlated on a segment-by-segment basis to determine an average value to set as the detection threshold for the subsequent step. In the authentication stage, a similar process is conducted. In order to simulate a faster authentication phase by a mobile system, only beats from the first 2-5 detected segments are averaged to form a testing template. The two templates are time normalized and then cross-correlated to produce a similarity score. The score is compared to the threshold learned in the enrollment phase and any correlation coefficients above the threshold are accepted as the target class, while others are rejected.

The performance of the one-class classifier for all data sets tested solely against subject 1 lies within in Table V, indicating that the subject was correctly identified with an accuracy of 95.89%. We next evaluate the classification performance of the remaining subjects, in the same manner as we did Subject 1, by using one recording from each subject set as the target class and all other recordings from the same subject and other subjects as test cases. These trials produced a classification accuracy above 97% for all subjects (Figure 17b), and a false positive rate not exceeding 2.6% (Figure 17a). The ECG authentication algorithm designed specifically for our application provides high accuracy and low false positive rate, similar to pre-existing algorithms,

This article has been accepted for publication in a future issue of this journal, but has not been fully edited. Content may change prior to final publication. Citation information: DOI 10.1109/TWC.2019.2921964, IEEE Transactions on Wireless Communications

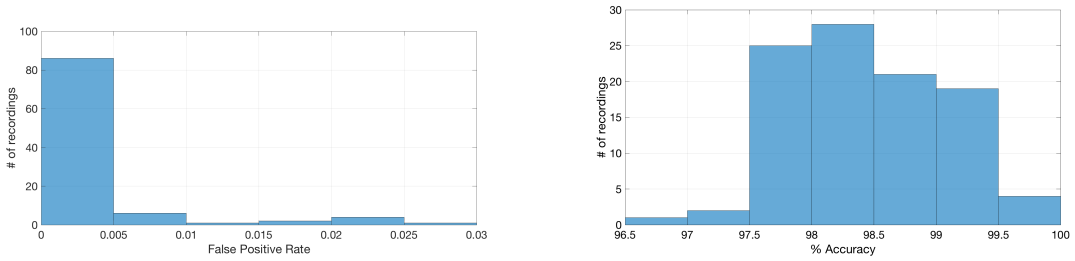

(a) ECG classification false positive rate of 100 recordings from 20 subjects

(b) ECG classification accuracy of 100 recordings from 20 subjects

Fig. 17: Statistical results of ECG classification

while offering low-complexity feature selection.

•**Performance Discussion:** The dominant source of confusion in the classification process comes from the lack of additional distinguishing features to support our correlation-based method. The dynamic threshold, in almost all cases, is set extremely high which causes a low false positive, but also degrades the true positive performance. Although results still generate a high classification accuracy and indicate strong potential to use ECG signals as a biometric, additional analysis must be undertaken to support the wide adoption of such a method. For this study in particular, an improvement in the false positive and true positive rate are necessary steps in ensuring classification stability. For future experiments, we seek to improve algorithm performance and provide experimental results that emphasize the limitations that exists in a real-time measurement scenarios. Specifically, we aim to conduct a large-scale measurement campaign where the ECG signals from multiple subjects are measured in real-time, an under ambulatory conditions where different physiological states can be observed [28].

REFERENCES

[1] M. Swaminathan, F. S. Cabrera, J. S. Pujol, U. Muncuk, G. Schirner, and K. R. Chowdhury, "Multi-path model and sensitivity analysis for galvanic coupled intra-body communication through layered tissue," *IEEE Transactions on Biomedical Circuits and Systems*, vol. 10, no. 2, pp. 339–351, April 2016.

[2] A. Pal, A. Kumar Gautam, and Y. Singh, "Evaluation of bioelectric signals for human recognition," vol. 48, pp. 747–753, 12 2015.

[3] A. Fratini, M. Sansone, P. Bifulco, and M. Cesarelli, "Individual identification via electrocardiogram analysis," in *Biomedical engineering online*, 2015.

[4] X. Zhai, A. Amira, and F. Bensaali, "Ecg security identification system on the zynq soc platform," in *2015 IEEE International Conference on Computer and Information Technology; Ubiquitous Computing and Communications; Dependable, Autonomic and Secure Computing; Pervasive Intelligence and Computing*, Oct 2015, pp. 1164–1169.

[5] "Nymi white paper." [Online]. Available: https://nymi.com/

[6] Z. Cai, M. Seyedi, W. Zhang, F. Rivet, and D. T. H. Lai, "Characterization of impulse radio intrabody communication system for wireless body area networks," *Journal of Medical and Biological Engineering*, vol. 37, no. 1, pp. 74–84, Feb 2017. [Online]. Available: https://doi.org/10.1007/s40846-016-0198-9

[7] M. H. Seyedi, *A Novel Intrabody Communication Transceiver for Biomedical Applications*, 2014. [Online]. Available: http://vuir.vu.edu.au/25847/

[8] H. Baldus, S. Corroy, A. Fazzi, K. Klabunde, and T. Schenk, "Human-centric connectivity enabled by body-coupled communications," *IEEE Communications Magazine*, vol. 47, no. 6, pp. 172–178, June 2009.

[9] T. Kang, K.-I. Oh, H. Park, and S. Kang, "Review of capacitive coupling human body communications based on digital transmission," *ICT Express*, vol. 2, no. 4, pp. 180 – 187, 2016, special Issue on Emerging Technologies for Medical Diagnostics. [Online]. Available: http://www.sciencedirect.com/science/article/pii/S2405959516301710

[10] K. Ito and Y. Hotta, "Signal path loss simulation of human arm for galvanic coupling intra-body communication using circuit and finite element method models," in *2015 IEEE Twelfth International Symposium on Autonomous Decentralized Systems*, March 2015, pp. 230–235.

[11] M. S. Wegmueller, M. Oberle, N. Felber, N. Kuster, and W. Fichtner, "Signal transmission by galvanic coupling through the human body," *IEEE Transactions on Instrumentation and Measurement*, vol. 59, no. 4, pp. 963–969, April 2010.

[12] M. Seyedi, Z. Cai, D. T. H. Lai, and F. Rivet, "An energy-efficient pulse position modulation transmitter for galvanic intrabody communications," in *2014 4th International Conference on Wireless Mobile Communication and Healthcare - Transforming Healthcare Through Innovations in Mobile and Wireless Technologies (MOBIHEALTH)*, 2014, pp. 192–195.

[13] C. Holz and M. Knaust, "Biometric touch sensing: Seamlessly augmenting each touch with continuous authentication," in *Proceedings of the 28th Annual ACM Symposium on User Interface Software & Technology*, ser. UIST '15. New York, NY, USA: ACM, 2015, pp. 303–312. [Online]. Available: http://doi.acm.org/10.1145/2807442.2807458

[14] M. Hessar, V. Iyer, and S. Gollakota, "Enabling on-body transmissions with commodity devices," in *Proceedings of the 2016 ACM International Joint Conference on Pervasive and Ubiquitous Computing*, ser. UbiComp '16. New York, NY, USA: ACM, 2016, pp. 1100–1111. [Online]. Available: http://doi.acm.org/10.1145/2971648.2971682

[15] N. Matsushita, S. Tajima, Y. Ayatsuka, and J. Rekimoto, "Wearable key: device for personalizing nearby environment," in *Digest of Papers. Fourth International Symposium on Wearable Computers*, Oct 2000, pp. 119–126.

[16] J. Yang and A. Sample, "Em-comm: Touch-based communication via modulated electromagnetic emissions," vol. 1, pp. 1–24, 09 2017.

[17] C. Y. M. N. W.J. Tomlinson, S. Banou and K. R. Chowdhury, "Secure on-skin biometric signal transmission using galvanic coupling," in *Proceedings of IEEE INFOCOM 2019*, 2019.

[18] A. Goldberg, L. Amaral, L. Glass, J. M. Hausdorff, P. C. Ivanov, R. Mark, J. E. Mietus, G. B. Moody, C.-K. Peng, E. Stanley, and et al., "Physiobank, physiotoolkit, and physionet: Components of a new research resource for complex physiologic signals," Mar 2018. [Online]. Available: https://www.ahajournals.org/doi/full/10.1161/circ.101.23.e215

[19] "Dielectric properties of body tissues." [Online]. Available: http://niremf.ifac.cnr.it/tissprop/

[20] B. Infantolino and J. Challis, "Architectural properties of the first dorsal interosseous," vol. 216, pp. 463–9, 04 2010.

[21] F. K. M., K. Sumiko, P.-T. Kia, and P. C. C., "Radial and ulnar cortical thickness of the second metacarpal," *Journal of Bone and Mineral Research*, vol. 10, no. 12, pp. 1930–1934. [Online]. Available: https://onlinelibrary.wiley.com/doi/abs/10.1002/jbmr.5650101212

[22] Y. Li, B. Bakkaloglu, and C. Chakrabarti, "A system level energy model and energy-quality evaluation for integrated transceiver front-ends," *IEEE Transactions on Very Large Scale Integration (VLSI) Systems*, vol. 15, no. 1, pp. 90–103, Jan 2007.

[23] I. Kuon and J. Rose, "Measuring the gap between fpgas and asics," *IEEE Transactions on Computer-Aided Design of Integrated Circuits and Systems*, vol. 26, no. 2, pp. 203–215, Feb 2007.

[24] J. Y. Hsieh, Y. C. Huang, P. H. Kuo, T. Wang, and S. S. Lu, "A 0.45-v low-power ook/fsk rf receiver in 0.18 μm cmos technology for implantable medical applications," *IEEE Transactions on Circuits and Systems I: Regular Papers*, vol. 63, no. 8, pp. 1123–1130, Aug 2016.

[25] J. Bae and H. J. Yoo, "The effects of electrode configuration on body channel communication based on analysis of vertical and horizontal electric dipoles," *IEEE Transactions on Microwave Theory and Techniques*, vol. 63, no. 4, pp. 1409–1420, April 2015.

[26] W. J. Tomlinson, F. Abarca, K. R. Chowdhury, M. Stojanovic, and C. Yu, "Experimental assessment of human-body-like tissue as a communication channel for galvanic coupling," in *2015 IEEE 12th International Conference on Wearable and Implantable Body Sensor Networks (BSN)*, June 2015, pp. 1–6.

[27] A. Molisch, "Channel sounding," in *Wireless Communication*, vol. 2, no. 8, 2015, pp. 145–152.

[28] S. Wahabi, S. Pouryayevali, S. Hari, and D. Hatzinakos, "On evaluating ecg biometric systems: Session-dependence and body posture," *IEEE Transactions on Information Forensics and Security*, vol. 9, no. 11, pp. 2002–2013, Nov 2014.